2024 IEEE International Conference on Robotics and Automation (ICRA 2024)
May 13-17, 2024. Yokohama, Japan

Fingertip Ultrasonic Array for Tactile Rendering

Jace Rozsa
Department of Electrical and Computer Engineering
Carnegie Mellon University
Pittsburgh, USA
jrozsa@andrew.cmu.edu

Sarah Costrell
Department of Mechanical Engineering
Carnegie Mellon University
Pittsburgh, USA
scostrel@andrew.cmu.edu

Melisa Orta Martinez
Robotics Institute
Carnegie Mellon University
Pittsburgh, USA
mortamar@andrew.cmu.edu

Gary K. Fedder
Department of Electrical and Computer Engineering
Carnegie Mellon University
Pittsburgh, USA
fedder@cmu.edu

***Abstract*—A miniature haptic stimulation device utilizes focused ultrasound to deliver a tactile haptic sensation to the finger. The 1-3 piezocomposite device has a 1 cm^2 footprint, which is an order of magnitude smaller than other ultrasonic haptic devices and is a good candidate for wearable tactile rendering systems. The device focuses energy to a 1 mm^3 voxel. The current prototype was validated with a small, preliminary human subject study and requires an average input voltage of 68.8 V to elicit tactile sensation. The sensory drive voltage threshold will decrease with future refinement of mechanical impedance matching and focusing.**

***Index Terms*—haptics, ultrasound, piezocomposite**

I. Introduction

Haptic technologies play a crucial role in many modern systems, from user electronics to virtual reality. In cooperative robotic applications, haptics is used to communicate important information to the user about the environment in which the robot is operating [1], [2]. This information is typically transmitted in two modes: kinesthetic (larger forces applied to the user which are felt in joints) and tactile (forces imparted to the skin, the focus of the current work). For tactile haptics, the device ideally is able to provide a stimulus without inhibiting the user's range of motion. In other words, tactile devices must be wearable. Therefore technologies that are lightweight, low-power, and small are desirable [3]. Additionally, the stimulus must be able to convincingly mimic real world surfaces and textures. These two requirements have proven challenging for current technologies [4].

Contemporary tactile devices are still far from recreating reality in a satisfactory manner [5], [6]. The majority of tactile stimulation technologies rely on actuators which impart a force to the skin through direct physical contact [7]–[11]. These actuators are typically worn on the finger along with the electrical components which drive the motors [6], [9], [12]. Hydraulic [13], shape memory [6], and vibrating motor [4] actuators have been incorporated into large-scale arrays and are used to simulate movement across the skin such as a caress. These devices typically incorporate individual actuators on the scale of millimeters to centimeters in size.

Such large individual actuators are bulky and awkward to wear [14]. Miniaturization challenges exist in scaling mechanical actuators into arrays for small areas like fingertips. Many actuators must be physically anchored in order to produce forces large enough to be sensed [9]. For wearable applications, this often places a limit on how small individual stimulators can be, as extra hardware for physical anchoring takes space. Actuation for haptics also suffers from problems of localizing the stimulus [10]. If one actuator is triggered it can often be felt in a larger area beyond the point of actuation. A spatially imprecise stimulation can reduce the effectiveness of haptic rendering.

As an alternative to mechanical actuators, ultrasonic waves can be used to stimulate tactile sensations [15]. In such applications, energy is transferred from the impinging wave to the surface of the skin through the acoustic radiation force [16], delivering a tactile sensation to the user. Mid-air ultrasonic haptic devices are a common application which exploits this mechanism [17], [18]. In such applications, a large array of ultrasonic transducers focuses ultrasonic power at a given point in space, typically using a phased array technique [19], [20]. A tactile sensation is felt when the focused ultrasonic waves impinge on the skin of the user. Because the frequency range of ultrasound is outside the sensitive range for human mechanoreceptors, the carrier signal must be modulated, either spatially or temporally, at frequencies under 1 kHz [9], [21]. In order to overcome the high attenuation of ultrasound in air, these devices are large (typically over 100 transducers are used, with each transducer having a footprint on the order of a square centimeter) and have high power requirements, with peak power consumption reaching 80 W for some systems [22].

One example of an attempt to remedy the limitations of operating in air involved placing ultrasonic transducers directly on the back of the hand, driving ultrasonic energy

979-8-3503-8457-4/24/$31.00 ©2024 IEEE

through the tissue and bone, and focusing to a point on the palm [23]. While this technique reduced power consumption, the device was still quite large and only capable of producing a single focal point on the hand at a time.

We present an ultrasonic haptic device that focuses ultrasound at the skin's surface using a piezocomposite phased-array transducer. The high efficiency of the piezocomposite transducer facilitates sufficient production of ultrasonic energy to stimulate a tactile sensation without requiring a large number of transducers. The device is an order of magnitude smaller than previous similar tactile haptic technologies [23]. It is lightweight and doesn't require physical anchoring. Additionally it delivers a spatially precise stimulus, making the proposed technology a good candidate for scaling to next generation skin-wearable haptic rendering systems. As a first experimental validation step, we quantify the efficacy of ultrasonic phased-array focusing on the skin and self-report the haptic effects of driving the device with a spatially uniform voltage.

II. Theory and Design

A. Ultrasonics

Gavrilov et al. in the 1970's performed a series of experiments on human subjects to assess perceived sensations of focused ultrasound as a function of ultrasonic frequency [24]. Table I, extracted from a later review publication [15], provides quantitative guidance on the ultrasonic pressure levels needed to arouse tactile, heat, and pain sensations in human fingertips. The threshold level varies between individuals and is also affected by modulation frequency [16].

In order to keep system power requirements down, it is imperative that the maximum amount of ultrasonic energy arrives at the target. One important source of loss in ultrasonic systems is energy reflection due to impedance mismatch [25]. The proportion of wave reflected when an incident wave is travelling normal to the material interface is:

$$\Gamma = \frac{Z_2 - Z_1}{Z_2 + Z_1} \tag{1}$$

where Z_1 and Z_2 are the acoustic impedances of the originating material and the target material, respectively. The piezoelectric material used for the transducer in the current application has an acoustic impedance of roughly 20 MRayl·s/m [26]. The acoustic impedance of human skin is around 1.5 MRayl·s/m [27]. This produces a reflection coefficient of -0.86, in other words, 86% of the acoustic wave incident upon this interface is reflected, only 14% is transmitted. A way to reduce this loss is to employ a matching material, as illustrated in Figure 1. While the approaches to impedance matching are many [25], we employ the simplest method of selecting a material with an acoustic impedance in between that of the target and originating material, where the optimal matching impedance is:

$$Z_{m,opt} = \sqrt{Z_2 Z_1} \tag{2}$$

which is 5.5 MRayl for the piezocomposite to skin case. In addition to selecting a material with the desired acoustic impedance, the reflected waves in the forward direction through the matching layer must constructively interfere by setting its thickness to an odd multiple of quarter wavelengths, i.e. $(2N+1)\lambda/4$, where integer $N \geq 0$. Neglecting attenuation loss in the matching material, the ratio of transmitted energy with to without the quarter-wave matching layer is then

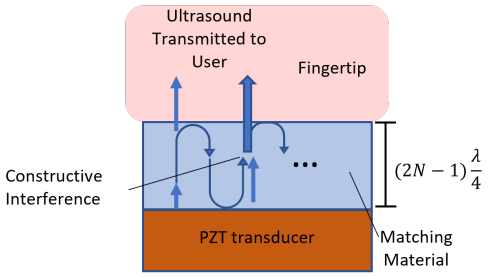

Fig. 1. Matching material and its effect on the ultrasound transmitted to the skin

$$\gamma = \left(\frac{4 Z_m Z_{skin}}{Z_m^2 + Z_{PZT} Z_{skin}} \right)^2 \frac{Z_{skin}}{Z_{PZT}} \tag{3}$$

In this instance we chose poly(methyl methacrylate) (PMMA), which has an acoustic impedance of 3.2 MRayl·s/m [28], as the matching material. This common polymer choice increases the transmitted energy by 2.9 times compared to no matching; however it is sub-optimal as it lowers the transmitted energy by around 24% of its maximum possible value.

B. Phased-Array Ultrasonic Focusing

Another method for increasing the pressure level at the user's skin is through phased array focusing. A simplified diagram of our 4×8 element phased array is shown in Figure 2 (a). In order to focus the ultrasound at point P, the drive signal applied to each transducer element is delayed such that output ultrasonic waves constructively interfere at P. This phase delay is

$$\psi_i = \frac{2\pi f}{v_p} \sqrt{(x_i - x_p)^2 + (y_i - y_p)^2 + (z_i - z_p)^2} \tag{4}$$

where f is the frequency of excitation, v_p is the speed of sound in the medium, and (x_i, y_i, z_i) and (x_p, y_p, z_p) are the center point of the element i in the array and the desired focal point, respectively.

C. Piezoelectric Transducer

The ultrasonic energy is produced using a piezoelectric transducer. The transducer material is a lead zirconate titanate (PZT) 5H2, 1-3 dice-and-fill piezocomposite (Smart Material Corp., Sarasota FL, USA). The piezocomposite is composed of high aspect ratio PZT pillars (125 µm x 125 µm x 1.5 mm) spaced 50 µm apart with epoxy between the pillars and thin-film metal electrodes deposited on opposing sides of the pillars (see Figure 2 (a)). In this particular case, the volume ratio of epoxy to PZT is 1:1. This unique

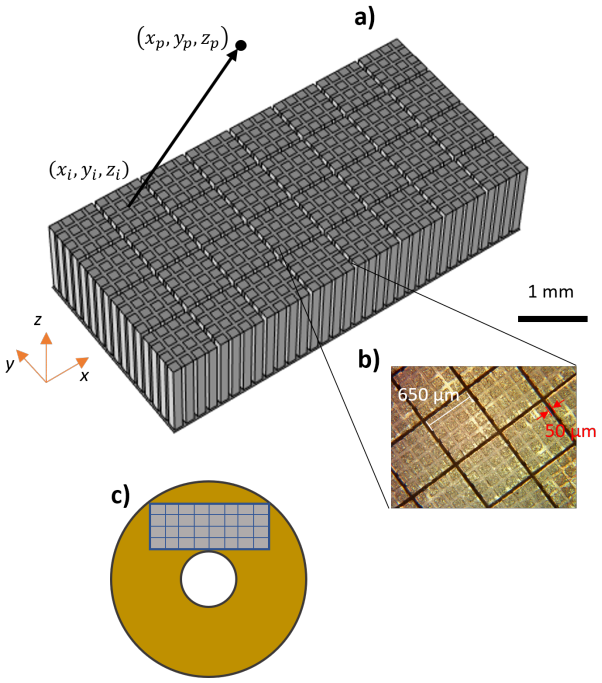

Fig. 2. Illustration of phased array focusing for present device, (a) diagram of piezocomposite phased-array, (b) image of actual piezocomposite with etched electrodes, (c) diagram of full material with phased array shaded in gray.

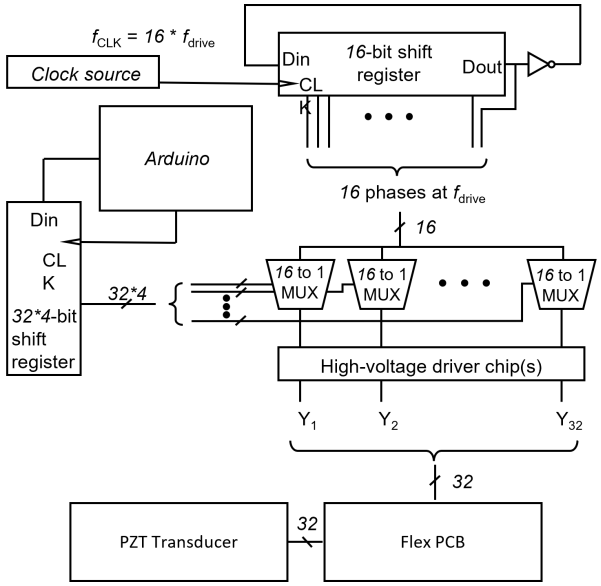

Fig. 3. Diagram of drive electronics

structure, as compared to a uniform PZT transducer, reduces the lateral modes at resonance and therefore increases the efficiency of the transducer. For this reason, piezocomposites are commonly employed in ultrasonic imaging systems [29].

Unlike in ultrasonic imaging applications, where resolution requires high signal bandwidth, tactile sensations occur at frequencies no higher than 400 Hz and so running haptic stimulation at high quality factor is advantageous. In order to maximize ultrasonic output, the transducer is driven at resonance in its fundamental piston mode. The corresponding resonance frequency is inversely proportional to the thickness of the piezocomposite (i.e. the pillar length). For the 1.5 mm thickness, the resonance is nominally 1 MHz.

III. Device Assembly and Experimental Results

A. Transducer Patterning

An ultrasonic phased array requires that each element be driven independently from the others. To this end, lithographic patterning and etching of the 2.5 µm thick copper-tin electrode on the top of the piezocomposite creates a uniform grid of electrically independent electrodes that aligns with the underlying PZT pillars. Each electrode in the grid connects a 4 × 4 sub-array of pillars to create individual and independent resonators with a pitch of 700 µm. A diagram and image of the etched piezocomposite are shown in Figure 2 (a) and (b), respectively. The footprint of the complete phased array is 5.5 mm × 2.8 mm. We also note that due to limited material availability, this phased array was patterned onto a piezocomposite material that was shaped like a disk, with inner and outer diameters of 2.5 mm and 10 mm, respectively (Figure 2(c)). While not ideal, only the 4 × 8 grid of electrodes was driven with a voltage signal. The effect of the rest of the idle material is minimal.

A flexible printed circuit board (PCB) with a 4 × 8 grid of electrodes mates to the etched electrodes of the piezocomposite. A device bonder aligned and assembled the PCB to the piezocomposite with electrical connections established with a flexible conductive epoxy (Epoxy Technology, EPO-TEK 78-134-5, Billerica MA, USA).

B. Experimental Setup

The drive electronics, shown in Figure 3, comprise a digital square wave generating board and an analog board that outputs signals 20 V in amplitude. These electronics boards generate 32 independent outputs, one for each element in the array, and have a phase resolution of $\pi/8$ radians.

Measuring individual pixel resonance using an impedance analyzer (Agilent 4294A) verified that all pixels functioned.

TABLE I
Ultrasonic threshold levels needed to achieve various tactile sensations [15]

Sensation	Tactile			Heat			Pain		
Frequency, MHz	0.48	0.887	1.95	0.48	0.887	1.95	0.48	0.887	1.95
Intensity, W/cm^2	8	15	80	55	90	1420	55	140	2860
Sound pressure, atm	4.9	6.7	15.5	13	16.5	65	13	21	93
Acoustic power, W	2.56	1.35	1.4	17.6	8.1	25	17.6	12.6	50

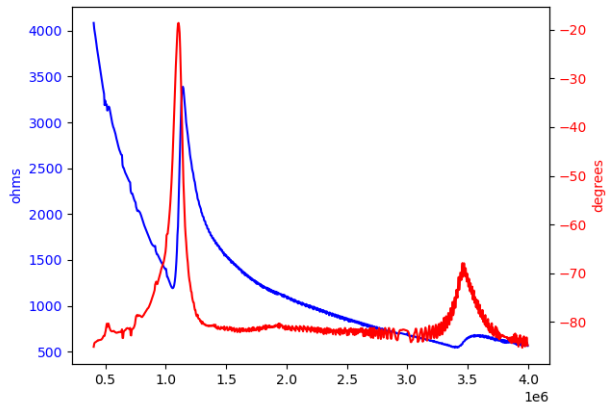

Fig. 4. Impedance spectrum of patterned piezocomposite transducer

The electrical impedance spectrum of the device with all pixels driven in parallel is shown in Figure 4. Resonance occurs at the dip in the impedance at 1.06 MHz. In order to experimentally verify the focusing capabilities of our device, we built a test setup, shown in Figure 5, to systematically measure the ultrasonic wavefront at precise locations in space. The setup comprised a 3D printer (MakerGear M2, Beachwood OH, USA) that was modified to hold a hydrophone (HGL-0085, Onda Corp., Sunnyvale CA, USA). The measurements were taken in water, which reduced the ultrasonic attenuation and minimized the input voltage requirement of the system. Additionally, the specific hydrophone used has an effective diameter of 85 µm, a size much smaller than the wavelength of the ultrasound in water (roughly 1.4 mm at 1 MHz). In order to produce ultrasonic waves in water, an open plastic container of water was placed on top of the transducer, with the electrically grounded side of the device in direct contact with a thin polyimide film sealing the bottom of the container. This polyimide film was 35 µm thick, far less than the ultrasonic wavelength by about a factor of 60, making it effectively invisible to the ultrasonic wave. Ultrasonic coupling gel (Aquasonic 100, Parker Laboratories, Fairfield NJ, USA) was applied to the transducer to eliminate air gaps between the device and the container. The hydrophone was immersed in the water from the open end of the container.

C. Validation of Phased Array Focusing

For validation of focusing in phased array operation, the coordinate system is chosen to match that of Figure 2. The focal point for the phased array was set 0.25 mm above the surface of the bottom of the plastic water container, and centered directly above the phased array. The transducer, described in section III-A, was driven at resonance. No matching material is placed between the device and the water tank.

Figure 6 shows the produced wavefronts measured with the hydrophone (note that this plot only contains amplitude information, not phase). In Figure 6(a), each element in the

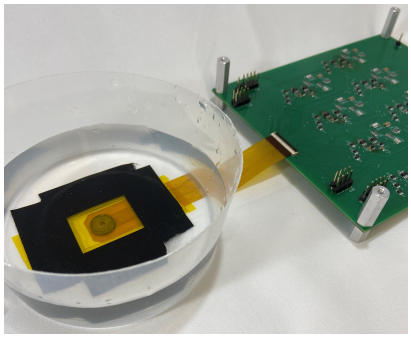

Fig. 5. Test setup used to acquire wavefront data with hydrophone.

array was driven with the same phase, producing a uniform plane wave. This plot acts as a baseline from which to compare the focusing plot. Figure 6(b) shows the result of driving each element in the array with a unique phase calculated so that the focal point occurs in the plane where the hydrophone is positioned. As can be seen from the plots, driving the transducer in the phased array configuration has a measurable effect on both the shape and amplitude of the resulting ultrasonic wavefront. Specifically, the amplitude is increased by about 20% when phased array focusing is implemented. Figure 7 shows how the focal point can be steered electronically. In this experiment, the phases were selected to produce a focal point off-center from the array.

D. Validation of Impedance Matching

The relationship between input voltage and pressure amplitude of the ultrasonic wave was established using the hydrophone setup described above. Using a high voltage

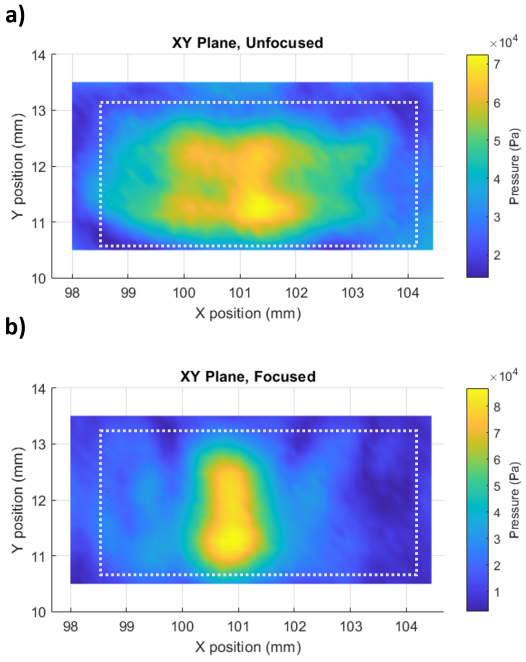

Fig. 6. Ultrasonic wavefronts produced by phased array in A) unfocused and B) focused drive configurations, white dotted line represents approximate outline of phased array

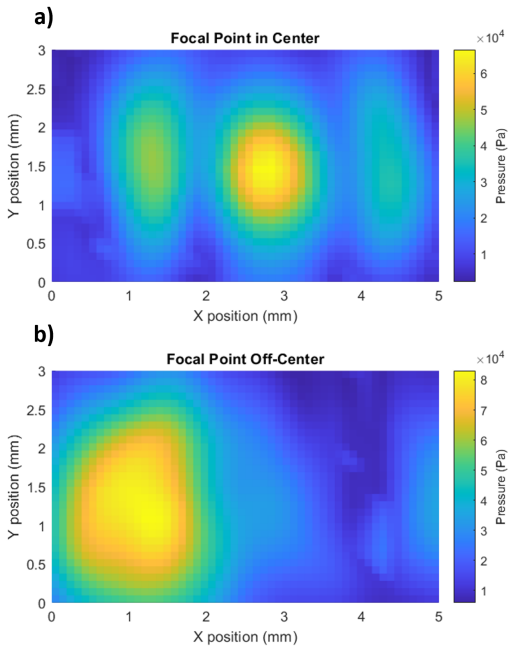

Fig. 7. Focal point in (a) center of array, and (b) shifted off-center due to alternative phase selection, highlighting the ability for the focal point to be steered. Data was gathered with a 1.0 mm needle hydrophone from Precision Acoustics, Dorchester, UK (note: the conditions of this experiment differ from that which produced the results of figure 6)

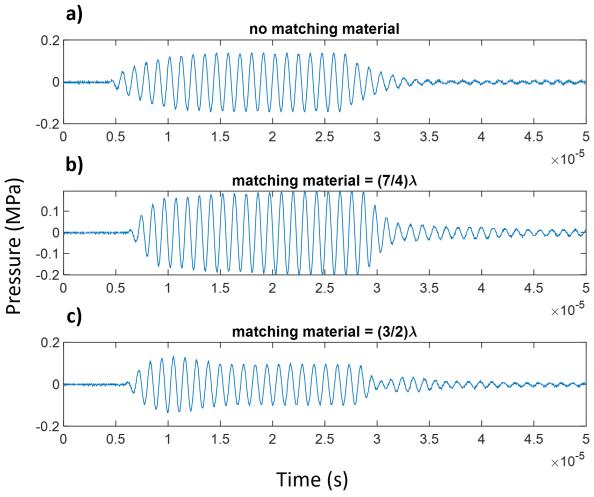

Fig. 8. Pressure waves measured in water for various matching configurations, steady-state values of 137, 189, and 101 kPa were observed for no matching material (a), quarter wavelength material (b), and half wavelength material(c), respectively.

amplifier (E&I 2100L, Electronics and Innovation LTD, Rochester NY, USA), we varied the input voltage from 11 V to 90 V and measured the resulting pressure amplitude. The relationship between voltage and pressure amplitude was linear with an R^2 value of 0.9998.

To validate the effect of the matching material, we took hydrophone measurements of the generated ultrasonic pressure wave with three different matching configurations: 1. no matching, 2. $\frac{3}{2}\lambda$ thickness matching material, and 3. $\frac{7}{4}\lambda$ matching material, with results shown in Figure 8. The transducer used in this instance differed from the patterned, phased array transducer described above. The material was 1.5 mm thick, with PZT pillars of 200 $\times$ 200 μm^2 footprint and 100 µm kerf, and a volume fill factor of 45%. The total size of the transducer was 12 mm $\times$ 12 mm, though only a 6 $\times$ 6 mm^2 quadrant was driven. The transducer was driven at resonance (900 kHz). For each of the tests, the hydrophone was placed roughly 0.5 mm from the bottom of the tank, and the transducer was driven with a uniform signal, i.e. with no phased-array focusing. Because the water in the plastic container is only a couple of inches deep, driving the transducer with a continuous wave results in interference between the waves entering the container and those reflecting off the water-air interface at the top of the tank causing a standing wave effect. A pulsed ultrasonic drive eliminates these measurement artifacts. Specifically, the transducer was driven for 20 µs, or roughly 20 drive cycles, so that by the time the reflected wave returns to the hydrophone from the top of the tank, the drive cycle is over and there is no incoming wave interference. As shown in Figure 8(b), adding the quarter-wave matching material increases the pressure amplitude by 40% relative to no matching material. In other words, the transmitted energy is increased by a factor of 1.9 (theory predicts an increase by a factor of 2.9). By contrast, the waveform from the $\frac{3}{2}\lambda$ matching, shown in Figure 8(c), indicates a decrease in the amplitude by 27% relative to no matching material, resulting in an energy attenuation factor of 0.54 (as opposed to a predicted factor of 0.66). In both cases, the transmitted energy was lower in experiment than in theory, suggesting that the the matching material is lossy. Furthermore, due to variations in the speed of sound in the matching material, the actual thickness of the matching material may not be exactly a quarter wavelength multiple, which would reduce the effect of constructive interference in the material.

E. Validation of Tactile Sensation

The ultrasound produced from a uniform excitation is capable of delivering tactile stimulation, despite the small size of the transducer. A small preliminary validation test was performed with the same transducer sample used to obtain the results of Figure 8. We performed a simple tactile threshold test, in which subjects were exposed to ever increasing levels of ultrasound until they reported a tactile sensation. The test ran as follows: with their finger placed on the PMMA matching material, and while viewing a graphical user interface displayed on a monitor, the subject was shown two consecutive screens, labeled 'Interval 1' and 'Interval 2", respectively. Each interval lasted 1 second. The device was turned on during one of the two intervals, and left off during the other. The interval at which the device was activated was selected randomly. The subject was then shown another screen where they were instructed to select in which interval the sensation was delivered. The subject could also select 'I don't know' or 'replay stimulus'. If the

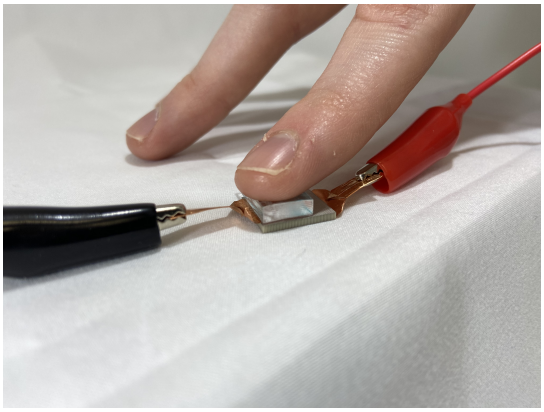

Fig. 9. Test setup used to verify haptic stimulation.

participant selected the wrong interval, or if they selected 'I don't know', the applied drive signal was increased by 10 volts. Once the participant selected the correct interval, the experiment was concluded and the tactile threshold was recorded as the voltage level at which the correct answer was given. For each of these tests, the drive signal was amplitude modulated at 200 Hz and the PMMA matching material had a thickness of $\frac{7}{4}\lambda$. In the setup, pictured in Figure 9, the transducer was driven with a high voltage using a power amplifier. Among the 4 people tested, all were able to feel a tactile sensation. The average tactile threshold was found at an input voltage of 68.8 V, with a standard deviation of 14.1 V. At the threshold voltage amplitude, the sensation was a faint vibratory tactile stimulus, according to those who participated in the preliminary study. Additionally, tests on the index finger of the authors at a much higher voltage, 240 V, resulted in a notable sensation that had various qualities which ranged from a fast vibration sensation, to a pin prick, to heat. We can infer from Figure 8(b) and the linearity of the pressure-voltage relationship that the ultrasonic pressure at the threshold voltage was on the order of 7 atm, which is in agreement with the threshold value predicted by the table in Table I.

IV. Conclusion

We have validated an ultrasonic haptic stimulator that is capable of focusing and steering ultrasonic energy to a 1 mm^3 voxel and has the potential for wearable haptic applications. Our self-reported tactile stimulation with the device in a non-focusing drive configuration provides justification for further refinement of this first prototype system.

While the voltage needed to produce a haptic sensation is high relative to CMOS electronic levels, we project the ability to get a reliable haptic sensation with 20% less voltage, or a signal of around 81 V with the addition of phased array focusing and refinement of matching. While still a high voltage level, it is not prohibitive for high-voltage CMOS drivers. Future work includes design of miniature electronics that can operate at this level, and can therefore produce high-pressure focused ultrasound. Additionally there is much to be learned about how the delivered ultrasonic haptic sensation is experienced by users. Further investigation of this phenomenon motivates future human subject studies.

V. Acknowledgements

The human subject study was performed under supervision of and with approval from the Carnegie Mellon University Institutional Review Board.

References

[1] J. A. Fishel, T. Oliver, M. Eichermueller, G. Barbieri, E. Fowler, T. Hartikainen, L. Moss, and R. Walker, "Tactile telerobots for dull, dirty, dangerous, and inaccessible tasks," in *2020 IEEE International Conference on Robotics and Automation (ICRA)*, 2020, pp. 11 305–11 310.

[2] M. Peshkin, J. Colgate, W. Wannasuphoprasit, C. Moore, R. Gillespie, and P. Akella, "Cobot architecture," *IEEE Transactions on Robotics and Automation*, vol. 17, no. 4, pp. 377–390, 2001.

[3] C. Pacchierotti, S. Sinclair, M. Solazzi, A. Frisoli, V. Hayward, and D. Prattichizzo, "Wearable haptic systems for the fingertip and the hand: Taxonomy, review, and perspectives," *IEEE Transactions on Haptics*, vol. 10, no. 4, pp. 580–600, 2017.

[4] E. Leroy, R. Hinchet, and H. Shea, "Multimode hydraulically amplified electrostatic actuators for wearable haptics," *Advanced Materials*, vol. 32, no. 36, p. 2002564, 2020. [Online]. Available: https://onlinelibrary.wiley.com/doi/abs/10.1002/adma.202002564

[5] D. Wang, Y. Guo, S. Liu, Y. Zhang, W. Xu, and J. Xiao, "Haptic display for virtual reality: progress and challenges," *Virtual Reality Intelligent Hardware*, vol. 1, no. 2, pp. 136–162, 2019. [Online]. Available: https://www.sciencedirect.com/science/article/pii/S2096579619300130

[6] N. Besse, S. Rosset, J. J. Zarate, and H. Shea, "Flexible active skin: Large reconfigurable arrays of individually addressed shape memory polymer actuators," *Advanced Materials Technologies*, vol. 2, no. 10, p. 1700102. [Online]. Available: https://onlinelibrary.wiley.com/doi/abs/10.1002/admt.201700102

[7] R. D. Howe, D. A. Kontarinis, W. J. Peine, and P. S. Wellman, "Tactile displays for increased spatial and temporal bandwidth in haptic feedback," in *Robotics Research*, Y. Shirai and S. Hirose, Eds. London: Springer London, 1998, pp. 269–277.

[8] J. Kim, B.-K. Han, D. Pyo, S. Ryu, H. Kim, and D.-S. Kwon, "Braille display for portable device using flip-latch structured electromagnetic actuator," *IEEE Transactions on Haptics*, vol. 13, no. 1, pp. 59–65, 2020.

[9] B. Hannaford and A. Okamura, *Haptics*, 01 2008, pp. 719–739.

[10] I. Gertler, G. Serhat, and K. J. Kuchenbecker, "Generating clear vibrotactile cues with a magnet embedded in a soft finger sheath," *Soft Robotics*, vol. 0, no. 0, p. null, 0, pMID: 36576497. [Online]. Available: https://doi.org/10.1089/soro.2021.0184

[11] S. Costrell, M. Alam, R. L. Klatzky, M. E. McHenry, L. M. Walker, and M. O. Martinez, "A magnetic soft device for tactile haptic actuation of the fingertip," in *2023 IEEE World Haptics Conference (WHC)*. IEEE, 2023, pp. 48–55.

[12] V. Vechev, J. Zarate, D. Lindlbauer, R. Hinchet, H. Shea, and O. Hilliges, "Tactiles: Dual-mode low-power electromagnetic actuators for rendering continuous contact and spatial haptic patterns in vr," Mar 2019.

[13] X. Yu, Z. Xie, Y. Yu, J. Lee, A. Vazquez-Guardado, H. Luan, J. Ruban, X. Ning, A. Akhtar, D. Li, B. Ji, Y. Liu, R. Sun, J. Cao, Q. Huo, Y. Zhong, C. Lee, S. Kim, P. Gutruf, C. Zhang, Y. Xue, Q. Guo, A. Chempakasseril, P. Tian, W. Lu, J. Jeong, Y. Yu, J. Cornman, C. Tan, B. Kim, K. Lee, X. Feng, Y. Huang, and J. A. Rogers, "Skin-integrated wireless haptic interfaces for virtual and augmented reality," *Nature*, vol. 575, no. 7783, pp. 473–479, Nov. 2019.

[14] R. P. Khurshid, N. T. Fitter, E. A. Fedalei, and K. J. Kuchenbecker, "Effects of grip-force, contact, and acceleration feedback on a teleoperated pick-and-place task," *IEEE Transactions on Haptics*, vol. 10, no. 1, pp. 40–53, 2017.

[15] L. R. Gavrilov and E. M. Tsirulnikov, "Focused ultrasound as a tool to input sensory information to humans (review)," *Acoustical Physics*, vol. 58, no. 1, pp. 1–21, Jan. 2012.

[16] D. Dalecki, S. Z. Child, C. H. Raeman, and E. L. Carstensen, "Tactile perception of ultrasound," *The Journal of the Acoustical Society of America*, vol. 97, no. 5, pp. 3165–3170, 1995.

[17] V. Shen, C. Shultz, and C. Harrison, "Mouth haptics in vr using a headset ultrasound phased array," in *Proceedings of the 2022 CHI Conference on Human Factors in Computing Systems*, ser. CHI '22. New York, NY, USA: Association for Computing Machinery, 2022. [Online]. Available: https://doi.org/10.1145/3491102.3501960

[18] T. Iwamoto, M. Tatezono, and H. Shinoda, "Non-contact method for producing tactile sensation using airborne ultrasound," in *Haptics: Perception, Devices and Scenarios*, M. Ferre, Ed. Berlin, Heidelberg: Springer Berlin Heidelberg, 2008, pp. 504–513.

[19] D. M. Plasencia, R. Hirayama, R. Montano-Murillo, and S. Subramanian, "Gs-pat: High-speed multi-point sound-fields for phased arrays of transducers," *ACM Trans. Graph.*, vol. 39, no. 4, aug 2020. [Online]. Available: https://doi.org/10.1145/3386569.3392492

[20] T. Hoshi, M. Takahashi, T. Iwamoto, and H. Shinoda, "Noncontact tactile display based on radiation pressure of airborne ultrasound," *IEEE Transactions on Haptics*, vol. 3, no. 3, pp. 155–165, 2010.

[21] E. Freeman and G. Wilson, "Perception of ultrasound haptic focal point motion," in *Proceedings of the 2021 International Conference on Multimodal Interaction*. New York, NY, USA: Association for Computing Machinery, 2021, p. 697–701. [Online]. Available: https://doi.org/10.1145/3462244.3479950

[22] I. Rakkolainen, E. Freeman, A. Sand, R. Raisamo, and S. Brewster, "A survey of mid-air ultrasound haptics and its applications," *IEEE Transactions on Haptics*, vol. 14, no. 1, pp. 2–19, 2021.

[23] D. Spelmezan, R. M. González, and S. Subramanian, "Skinhaptics: Ultrasound focused in the hand creates tactile sensations," in *2016 IEEE Haptics Symposium (HAPTICS)*, 2016, pp. 98–105.

[24] L. R. Gavrilov and E. M. Tsirulnikov, *Focused ultrasound in Physiology and Medicine*. Nauka, Leningrad [in Russian], 1980.

[25] V. T. Rathod, "A review of acoustic impedance matching techniques for piezoelectric sensors and transducers," *Sensors*, vol. 20, no. 14, 2020. [Online]. Available: https://www.mdpi.com/1424-8220/20/14/4051

[26] Smart Material Corporation. [Online]. Available: smart-material.com

[27] C. Kuhn, F. Angehrn, O. Sonnabend, and A. Voss, "Impact of extracorporeal shock waves on the human skin with cellulite: A case study of an unique instance," *Clinical interventions in aging*, vol. 3, pp. 201–10, 02 2008.

[28] J. Carlson, J. van Deventer, A. Scolan, and C. Carlander, "Frequency and temperature dependence of acoustic properties of polymers used in pulse-echo systems," in *IEEE Symposium on Ultrasonics, 2003*, vol. 1, 2003, pp. 885–888 Vol.1.

[29] Z. Han, N. Wang, Z. Li, X. Zhu, Y. Chen, X. Jian, and Y. Cui, "Phased-array transducer for intracardiac echocardiography based on 1–3 piezocomposite," *Frontiers in Materials*, vol. 8, 2021. [Online]. Available: https://www.frontiersin.org/articles/10.3389/fmats.2021.663926